Portosystemic shunting and persistent fetal vascular structures in aryl hydrocarbon receptor-deficient mice

Garet P. Lahvis*, Susanne L. Lindell†, Russell S. Thomas*, Robert S. McCuskey‡, Christopher Murphy§, Edward Glover*, Michael Bentz†, James Southard†, and Christopher A. Bradfield*¶

*McArdle Laboratory for Cancer Research, University of Wisconsin Medical School, Madison, WI 53706; †Department of Surgery, University of Wisconsin, Madison, WI 53792; ‡Department of Cell Biology and Anatomy, College of Medicine, University of Arizona, Tucson, AZ 85724-5044; and §Department of Surgical Sciences, School of Veterinary Medicine, University of Wisconsin, Madison, WI 53706

Edited by Allan H. Conney, Rutgers, State University of New Jersey, Piscataway, NJ, and approved July 10, 2000 (received for review June 5, 2000)

A physiological examination of mice harboring a null allele at the aryl hydrocarbon (*Ah*) locus revealed that the encoded aryl hydrocarbon receptor plays a role in the resolution of fetal vascular structures during development. Although the aryl hydrocarbon receptor is more commonly studied for its role in regulating xenobiotic metabolism and dioxin toxicity, a developmental role of this protein is supported by the observation that *Ah* null mice display smaller livers, reduced fecundity, and decreased body weights. Upon investigating the liver phenotype, we found that the decrease in liver size is directly related to a reduction in hepatocyte size. We also found that smaller hepatocyte size is the result of massive portosystemic shunting in null animals. Colloidal carbon uptake and microsphere perfusion studies indicated that 56% of portal blood flow bypasses the liver sinusoids. Latex corrosion casts and angiography demonstrated that shunting is consistent with the existence of a patent ductus venosus in adult animals. Importantly, fetal vascular structures were also observed at other sites. Intravital microscopy demonstrated an immature sinusoidal architecture in the liver and persistent hyaloid arteries in the eyes of adult *Ah* null mice, whereas corrosion casting experiments described aberrations in kidney vascular patterns.

The aryl hydrocarbon receptor (AHR) is a member of the per-arnt-sim (PAS) superfamily of proteins. The AHR regulates biological responses to a variety of environmental contaminants, such as the polycyclic aromatic hydrocarbons found in cigarette smoke, the polychlorinated dioxins that contaminate industrial chemicals, and the wartime defoliant Agent Orange (1–5). These chemical ligands bind to the AHR, leading to receptor dimerization with another PAS protein known as the aryl hydrocarbon nuclear translocator (ARNT). This heterocomplex interacts with genomic enhancer elements upstream of a battery of target genes that encode xenobiotic metabolizing enzymes (1, 6, 7). The observation that the up-regulated enzymes often have metabolic activity toward AHR agonists has led to the idea that this pathway represents an adaptive metabolic response that protects an organism from exposure to certain classes of toxic environmental contaminants. Although this adaptive role has considerable experimental support, this pathway is not always protective. Exposure to high-affinity AHR agonists, like the chlorinated dioxins, can result in cancer (8), immunosuppression (9), liver damage (10), and birth defects (11). The mechanisms underlying these toxic effects are unknown but appear to be AHR mediated.

Because of its role in mediating responses to environmental contaminants, the biology of the AHR has been extensively characterized from a toxicological viewpoint. However, several observations suggest an additional role for the AHR in vertebrate development. First, a phylogenetic survey indicates that the AHR arose over 450 million years ago, with functional orthologs found in species that have evolved in various marine, aquatic, and terrestrial environments (12). This observation suggests that the AHR has conferred a selective advantage throughout vertebrate evolution, in a variety of chemical environments and before environmental pollution by anthropogenic compounds. Second, the AHR is expressed in a variety of tissues and developmental time points that are inconsistent with a singular role as part of a metabolic defense against environmental chemicals (13–15). Finally, mice that lack the aryl hydrocarbon (*Ah*) locus (*Ah* −/−) were generated by different laboratories and provided preliminary evidence that the AHR could affect reproduction, survival, and growth (16–20). The intent of the present study was to obtain a physiological explanation for the phenotype observed in *Ah* −/− mice and to identify a common receptor-related process that could provide insights into the role of the AHR in vertebrate development.

Materials and Methods

Mice. *Ah* −/− mice congenic to C57BL/6J (B_6) were generated by 15 backcrosses (N15) to the B_6 background with continual selection for the *Ah* null allele. *Ah* +/+ mice were derived from matings of N15 *Ah* heterozygous null (+/−) mice. Mice were then intercrossed to generate a colony of *Ah* −/−, +/−, and +/+ mice. The *Ah* −/− mice are maintained by intercrossing.

Morphometry. Livers were fixed in formalin, and 6-μm sections were examined after staining with hematoxylin/eosin. Nuclear and cytoplasmic areas were determined by a point-count-intersect method (21). Intersect points were categorized as hepatocyte nucleus, hepatocyte cytoplasm, or other (e.g., sinusoid or erythrocyte). The hepatocellular area was determined by dividing the total grid area by the number of nuclei within the grid. Nuclear and cytoplasmic areas were calculated by multiplying the total hepatocellular area by nuclear cytoplasmic densities.

Colloidal Carbon Uptake. Mice were anesthetized via inhalation of methoxyfluorane (Schering-Plough Animal Health), and their abdominal wall was surgically incised to expose the liver. The portal vein was cannulated with a 24-gauge angiocatheter (Bec-

This paper was submitted directly (Track II) to the PNAS office.

Abbreviations: *Ah*, aryl hydrocarbon; AHR, *Ah* receptor; PAS, per-arnt-sim; ARNT, *Ah* nuclear translocator; DV, ductus venosus; IVC, inferior vena cava; SJF, sinusoidal junctions per field.

¶To whom reprint requests should be addressed at: McArdle Laboratory for Cancer Research, 1400 University Avenue, Madison, WI 53706-1599. E-mail: bradfield@oncology.wisc.edu.

The publication costs of this article were defrayed in part by page charge payment. This article must therefore be hereby marked "*advertisement*" in accordance with 18 U.S.C. §1734 solely to indicate this fact.

Article published online before print: *Proc. Natl. Acad. Sci. USA*, 10.1073/pnas.190256997. Article and publication date are at www.pnas.org/cgi/doi/10.1073/pnas.190256997

ton Dickinson), and the suprahepatic vena cava was incised. The liver was flushed with 10 ml of Krebs–Henseliet bicarbonate buffer from a height of 30 cm to remove blood cells before excision and weighing. To relax postoperative vasoconstriction, perfusion was held at a constant flow rate of 3 ml/g/min with Krebs–Henseliet bicarbonate buffer, at an O_2 concentration of 95% and a CO_2 concentration of 5%, with a constant temperature of 25°C for 10 min (22). After isolated perfusion, the liver was flushed with 10 ml of colloidal carbon (Pelican Ink), which was prepared by extensive dialysis (48 h), and filtered through an 8-μm mesh (22).

Corrosion Casts. Mice were anesthetized and livers were flushed with 10 ml of Krebs–Henseliet bicarbonate buffer, as above. Methylmethacrylate resin was prepared according to the protocol recommended by the manufacturer (Polysciences). Briefly, 20 ml of methylmethacrylate monomer was mixed with three drops of promoter and approximately 0.5 ml of dye and stored on ice. A second mixture of monomer (3.5 ml) and catalyst (1.0 ml) was made before each injection and was then mixed thoroughly with an equal volume of the promoter resin and injected. Livers were perfused via cannulation of the portal vein at a constant rate of 150 μl/min with a syringe pump (Harvard Apparatus), and the inferior vena cava (IVC) was incised to allow for resin outflow. Livers were also perfused with resin by cannulation of the infrahepatic IVC and occlusion of the suprahepatic IVC, with outflow through the incised portal vein. Kidneys were also perfused retrograde by cannulation of the IVC below the renal vein and occlusion of the infrahepatic IVC between the kidney and liver. Resin flowed from the kidney through the renal artery and out the descending aorta. After perfusion, resin was allowed to harden for 30 min, and organs were then digested with 20% potassium hydroxide for 48 h at 25°C.

Intravital Microscopy. Mice were anesthetized via i.p. injection of urethane (10 mg/kg) (Sigma), and the abdominal wall was incised. The left lobe of the liver was exposed, covered with Saran wrap, and transilluminated at 550–680 nm. A modified Leitz microscope with 10×, 20×, and water immersion 80× objectives was used to obtain images of the liver. Images were recorded on videotape with a silicon-vidicon camera (23). Internal diameter, the number of sinusoids containing blood flow, and the number of sinusoidal junctions per field (SJF) were determined in blinded studies of individual fields obtained with the 80× objective.

Portal-Systemic Shunting. The portal vein was cannulated with a 24-gauge angiocatheter, and the left ventricle was incised. The liver was flushed with 10 ml of PBS from a height of 30 cm and then perfused at a constant rate of 1 ml/min with 150,000 gold microspheres (15-μm diameter) per milliliter of PBS (BioPhysics Assay Laboratory, Worcester, MA) for 5.5 min. Livers and lungs were perfused, excised, and then dried at 50°C overnight. The number of microspheres in each sample was quantified by neutron activation of the gold microspheres and subsequent counting of γ radiation (BioPhysics Assay Laboratory). The extent of portosystemic shunting was calculated with the following formula (24): PSS% = (number of microspheres in lung/number of microspheres in lung and liver) × 100.

Angiography. Continuous x-ray images were obtained as contrast was injected into the portal veins of *Ah* +/+ and *Ah* −/− mice. Continuous images were obtained over approximately 10 s with an OEC 9800 Portable Vascular C-ARM (Medical Systems, Salt Lake City, UT), with injection of approximately 1 ml of Omnipaque 300 (Nycomed, Princeton, NJ) postmortem into the hepatic portal vein.

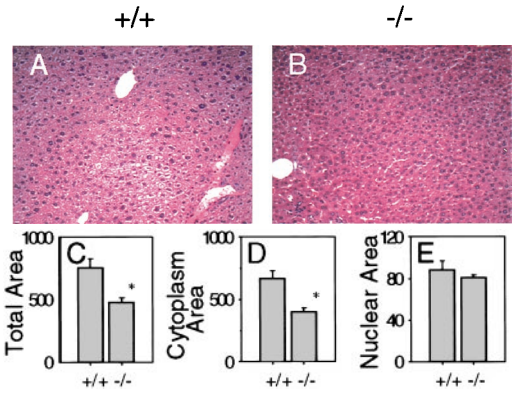

Fig. 1. *Ah* −/− mice have smaller hepatocytes than wild-type mice. Livers of 1-year-old mice were fixed in formalin, and 6-μm sections were examined after staining with hematoxylin/eosin. (*A* and *B*) Thin sections from wild-type (*A*) and age-matched *Ah* knockout (*B*) mice are shown, and results of morphometric analyses follow. (*C*) There is a significant decrease in the total area of the hepatocytes of *Ah* −/− mice. (*D* and *E*) Whereas the cytoplasmic area of *Ah* −/− hepatocytes is significantly decreased (*D*), the nuclear areas of *Ah* +/+ and *Ah* −/− hepatocytes are not different (*E*). Mean and standard errors generated from comparison of six 1-year-old male *Ah* +/+ and six age- and sex-matched *Ah* −/− mice are shown; asterisks indicate significance ($P < 0.05$).

Examination for Hyaloid Artery and Limbal Vasculature. Eyes were dilated with two applications of 1% tropicimide (Bausch and Lomb) and examined with a hand-held biomicroscope (Kowa SL2). Structures examined include the eyelids, cornea, iris, anterior chamber, lens, and anterior vitreous. Eyes were also evaluated by indirect and direct ophthalmoscopy for hyaloid structures. To compare groups, we evaluated 15 *Ah* +/+ and 14 *Ah* −/− mice. The observer was blinded to genotype; the degree of hyaloid artery persistence was scored as follows: 0 = no hyaloid artery present, 1 = Bergmeister papilla or slight extension of hyaloid artery into posterior vitreous, 2 = extensive hyaloid vessel development extending at least one-quarter of the distance to the lens and up to the posterior lens capsule. The score assigned to each animal was based upon the eye with the more extended artery. Results were statistically evaluated by using the two-tailed Fisher's exact test (25). To provide histological sections defining the extended hyaloid artery, eyes were

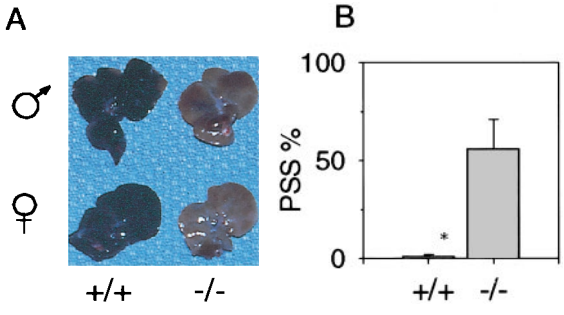

Fig. 2. (*A*) Livers of *Ah* −/− mice exhibit portosystemic shunting. With perfusion of colloidal carbon, livers of *Ah* +/+ mice become black (*Left*), whereas livers of *Ah* −/− mice remained pink (*Right*). The livers of male mice are shown above the livers of female mice. The figure represents livers of five male and five female mice from each group. (*B*) In *Ah* −/− mice, microspheres bypass liver sinusoids. The hepatic portal veins of six *Ah* +/+ and 6 *Ah* −/− mice were injected with microspheres and then livers and lungs were removed. The extent of portosystemic shunting was calculated as the number of microspheres found in lung divided by the number of microspheres found in both the lung and the liver. Mean and standard errors are shown; asterisks indicate significance ($P < 0.05$).

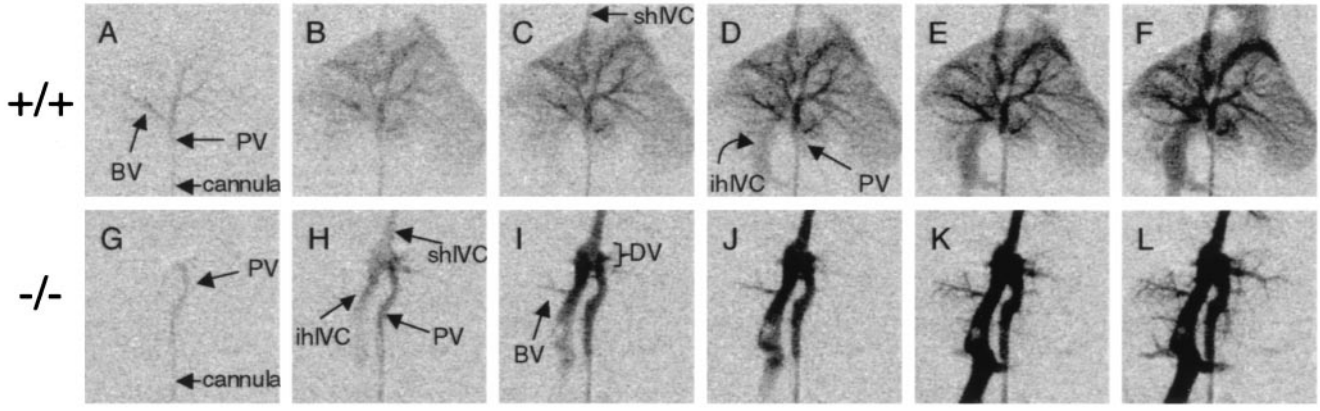

Fig. 3. Angiography indicates patent ductus venosus. Continuous x-ray images were obtained over approximately 10 s as contrast was injected into the portal veins of *Ah* +/+ (*A–F*) and *Ah* −/− (*G–L*) mice. Angiograms are representative for five *Ah* +/+ and five *Ah* −/− mice. Serial radiographs are presented from left to right, showing the portal vein (PV), infrahepatic inferior vena cava (ihIVC), suprahepatic inferior vena cava (shIVC), ductus venosus (DV), and branching vessels (BV).

fixed in 10% buffered formalin, sectioned, and stained with Alcian Blue PAS. Limbal vessels were photographed after mice were injected with 200 μl of 0.05 g fluorescein isothiocyanate-dextran (Sigma)/ml of PBS, and eyes were epi-illuminated at 488 nm.

Results

Smaller *Ah* −/− Liver Weights Reflect a Reduced Portal Blood Supply. In our hands, the most reproducible phenotype found in *Ah* −/− mice is a 25% reduction in relative liver weight (16, 17, 19, 26, 27), with no significant hepatopathology in adult animals (17, 19). Given that the set point for liver weight is highly regulated (28–30), we chose to elucidate the etiology of this biological endpoint. Although microscopic evaluation of hematoxylin/eosin sections did not provide significant insight into the reduced liver size (Fig. 1 *A* and *B*), examination of cell size by direct morphometric analysis revealed that hepatocytes from *Ah* −/− mice were 35% smaller in total cellular area than were hepatocytes from wild-type littermate controls (Fig. 1*C*). The cytoplasmic area of hepatocytes from *Ah* −/− mice was decreased in size by nearly 50% (Fig. 1*D*), but nuclear areas were not significantly different (Fig. 1*E*). Thus, the reduced size of the livers in *Ah* −/− mice reflects a decrease in hepatocyte size, primarily from reduced cytoplasmic volume.

Because it is known that relative liver weight and hepatocyte size decrease in response to starvation or to introduction of portosystemic shunts (shunts from the portal vein to the IVC) (31–34), we suspected that there was an alteration in the liver vasculature of *Ah* −/− mice that was not apparent in hematoxylin/eosin-stained histological sections (Fig. 1 *A* and *B*). Thus, we examined intrahepatic vascularity by *in situ* perfusion approaches. In the first experiment, we measured colloidal carbon uptake in isolated perfused livers. Upon perfusion of colloidal carbon into wild-type livers from the portal vein, the regions at the base of the lobes immediately turned black, with carbon coloration spreading toward the periphery of the lobe, completely filling the liver within 3 min. In contrast, *Ah* −/− livers remained pink throughout the carbon flush for periods of more than 10 min, despite carbon flow out of the IVC (Fig. 2*A*). This drastic reduction in filling of the hepatic vasculature with colloidal carbon was observed among all *Ah* −/− mice, regardless of sex or age, whereas carbon filled the lobes of all matched *Ah* +/+ mice. Inadequate carbon filling was observed among *Ah* −/− mice that were 21 days of age and over a year in age (data not shown). Colloidal carbon uptake was not increased in the *Ah* −/− liver with the concomitant perfusion of vasodilators, such as sodium nitroprusside (10^{-5} M), verapamil HCl (10^{-6} M), or the endothelin-1 receptor antagonist PD142893 (10^{-5} M) (data not shown). Based on these results, we concluded that the decreased perfusion of *Ah* −/− livers was due to a difference in vascular morphology rather than vasoconstriction.

A possible reason for the poor carbon uptake of *Ah* −/− livers was the existence of portosystemic shunting. To assess this possibility, we injected gold microspheres of 15-μm diameter into the portal vein and incised the left ventricle of the heart, allowing microspheres that were not trapped in the liver sinu-

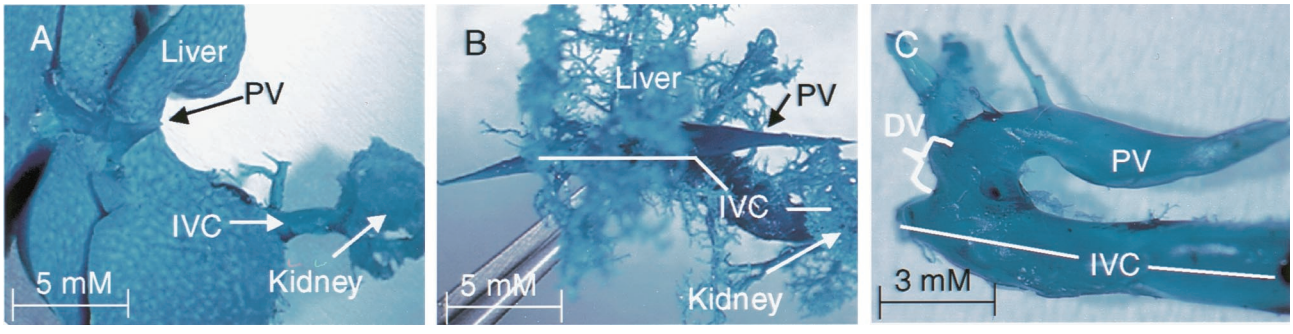

Fig. 4. Corrosion casts provide a three-dimensional image of putative ductus venosus in *Ah* −/− mice. The portal vein (PV), inferior vena cava (IVC), and ductus venosus (DV) are shown in corrosion casts of wild-type (*A*) and congenic age-matched *Ah* −/− (*B* and *C*) livers. Corrosion casts are representative of at least six *Ah* +/+ and six *Ah* −/− mice. The cast in *C* shows the patent DV from an *Ah* −/− mouse after individual vessel branches were removed.

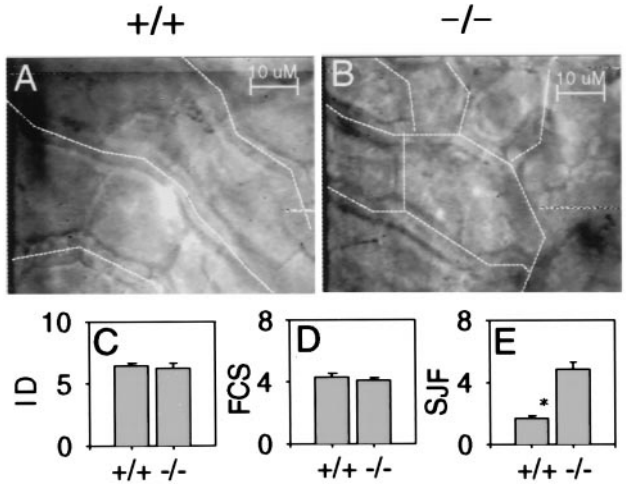

Fig. 5. Sinusoids of *Ah* −/− mice are more anastomotic than those of *Ah* +/+ mice. Still images from 80× water immersion objectives were collected from videotapes of intravital microscopy of *Ah* +/+ (*A*) and *Ah* −/− (*B*) livers. Sinusoids are identified with dotted lines, as they not as readily visible in individual frames as compared with videotapes. A comparison of the internal diameter of individual sinusoids (ID), the number of flow-containing sinusoids (FCS), and the number of sinusoidal junctions per field (SJF) is shown (*C–E*, respectively) as mean and standard error. For ID and FCS, 28 and 18 fields were examined from four *Ahr* +/+ and three *Ahr* −/− livers, respectively. For SJF, 20 and 15 fields from three *Ahr* +/+ and three *Ahr* −/− livers were examined, respectively.

soids (approximately 6–7-μm internal diameter) to flow through the right side of the heart and collect in the lung. We quantified the portosystemic shunting by comparing the number of microspheres that accumulate in liver sinusoids with the number that bypass the sinusoids via shunts and collect in the lungs (24). More than half (56.1%) of the microspheres passed through the *Ah* −/− livers, whereas only 1.0% passed through the wild-type livers (Fig. 2*B*). These results demonstrated that portal blood flow to hepatocytes via the sinusoidal compartment was significantly reduced ($P < 0.013$). Also consistent with significant portosystemic shunting in *Ah* −/− mice was the finding that resistance to perfusion of the liver through the portal vein at a constant flow rate was not significantly greater in *Ah* −/− mice relative to wild-type controls (range: 6–14 mm Hg; data not shown).

The AHR Is Required for Resolution of the Ductus Venosus (DV). To determine the nature of the portosystemic shunt, we collected serial angiograms to observe the flow of contrast medium through the perfused liver. In wild-type mice, contrast medium flowed into the portal vein and immediately into the portal branches of the liver (Fig. 3*A*). After filling the major branching veins, contrast entered the suprahepatic IVC (Fig. 3*C*) and then flowed retrograde, filling the infrahepatic IVC (Fig. 3*D*). However, contrast medium in both male and female *Ah*−/− mice flowed from the portal vein directly to the IVC. Contrast filled the IVC first (Fig. 3*H*) and only slowly filled the individual branches of the liver (Fig. 3 *I–L*). The shunt between the portal vein and the IVC in the *Ah*−/− mouse was clearly visible as a short segment that runs perpendicular to both the portal vein and IVC within the liver. This vascular pattern is consistent with a patent DV (35). This fetal vascular structure is a remnant of fetal circulation and typically resolves shortly after parturition.

To obtain a three-dimensional reconstruction of the shunt, we perfused the portal vein with a methylmethacrylate resin and then digested away the cellular material with potassium hydroxide to provide a "corrosion cast" of the hepatic vasculature. The casts from the livers of wild-type mice appeared grossly as a solid mass of resin, indicating that resin perfused through the entirety of hepatic sinusoids before flow out to the IVC (Fig. 4*A*). The portal vein is clearly visible entering the liver (Fig. 4*A*) and the IVC can be seen on the dorsal side of the liver (data not shown). In contrast, resin in all *Ah* −/− livers did not perfuse the sinusoids and was limited to portal veins of each lobe and their primary and secondary branches (Fig. 4*B*). This pattern of vascular filling in the *Ah* −/− liver was also observed when the resin was injected retrograde into the liver from the IVC through the hepatic central veins (data not shown). Incomplete filling of the *Ah* −/− liver was explained by the presence of a shunt within the corrosion casts, which can be seen more clearly when branch vessels into the liver are removed (Fig. 4*C*). As with the angiogram, the direction of the shunt is perpendicular to that of the portal vein and IVC and is indicative of a patent DV.

Neonatal Sinusoidal Patterns Are Not Resolved in *Ah* −/− Mice. Portosystemic shunting can result from increased intrahepatic resistance to blood flow (36). To determine if the microcirculation of the *Ah* −/− liver impeded blood flow, we examined sinusoidal diameter and density, using intravital microscopy and real-time video imaging (for a review, see ref. 23). From different microscopic fields (Fig. 5 *A* and *B*), we observed that neither the internal diameter (Fig. 5*C*) nor the density of the sinusoids (Fig. 5*D*) differed between *Ah* null and wild-type mice. Despite normal sinusoidal density, we did observe that the sinusoidal pattern in *Ah* −/− mice resembles the neonatal architecture before resolution of the sinusoidal junctions during liver development (37). Sinusoids of wild-type mice were organized as

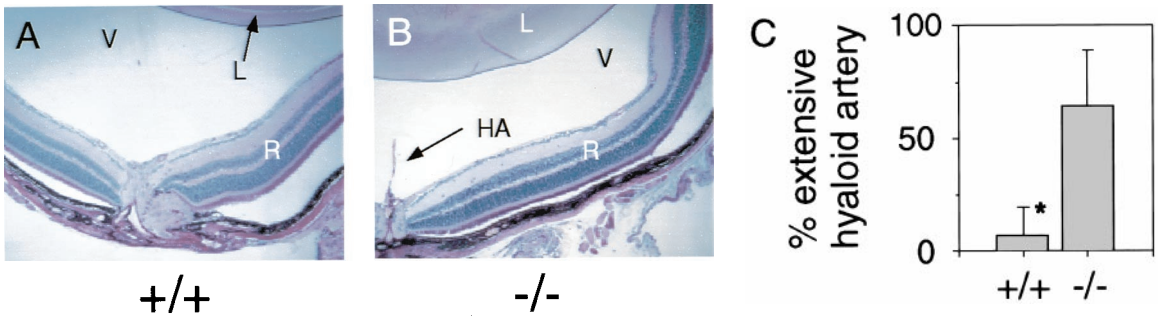

Fig. 6. *Ah* −/− mice have a high incidence of persistent hyaloid artery. To provide histological sections defining the extended hyaloid artery, eyes of *Ah* +/+ (*A*) and *Ah* −/− (*B*) were fixed in 10% buffered formalin and 6-μm sections were stained with Alcian Blue PAS. The lens (L), vitreous (V), retina (R), and hyaloid artery (HA) are shown. Eyes of *Ah* +/+ and *Ah* −/− mice were examined by indirect and direct ophthalmoscopy for hyaloid structures; a graph of hyaloid artery persistence is shown (*C*). The difference between *Ah* +/+ *and Ah* −/− mice was significant ($P < 0.005$), and the percentage of mice with extensive hyaloid artery is shown with the 95% upper confidence internal. Results were statistically evaluated by using the two-tailed Fisher's exact test (25).

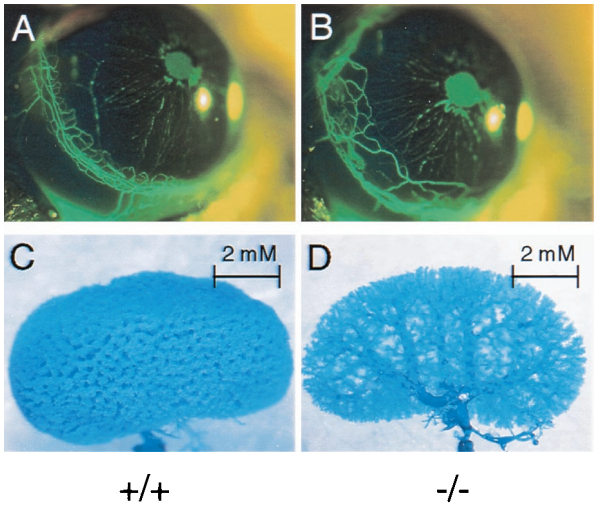

Fig. 7. *Ah* −/− mice have expansion of limbal vessels and altered kidney vascular structure. (*A* and *B*) Limbal vessel structures of *Ah* +/+ (*A*) and *Ah* −/− (*B*) mice are shown. Limbal vessels were photographed after nine *Ah* +/+ and nine *Ah* −/− mice were injected with fluorescein isothiocyanate-dextran, and eyes were epi-illuminated at 488 nm. (*C* and *D*) Corrosion casts of kidney vasculature of *Ah* +/+ (*C*) and −/− (*D*) mice are also shown and are representative of at least four mice from each group.

parallel vessels in the centrilobular regions, whereas sinusoids in *Ah* −/− mice were highly anastomotic throughout (Fig. 5 *A* and *B*). When quantified by a count of SJF, sinusoidal anastomoses were found to be significantly higher among *Ah* −/− livers (4.8 SJF) as compared with livers from wild-type mice (1.7 SJF, $P < 0.0026$) (Fig. 5*E*).

***Ah* −/− Mice Exhibit Vascular Anomalies in the Eye and Kidney.** Evidence for fetal vascular structures in the liver led us to search for similar structures at other sites. Remnants of neonatal architecture were also found in the eyes of *Ah* −/− mice. When eyes of 8- to 12-week-old *Ah* −/− mice were examined by ophthalmoscopy, they were commonly found to contain a persistent hyaloid artery (Fig. 6*B*). This fetal artery supplies the developing eye with blood. Of 14 *Ah* −/− mice, nine exhibited an extensive hyaloid artery, whereas only 1 of 15 *Ah* +/+ mice exhibited this structure (Fig. 6*C*). In 25% of *Ah* −/− mice, the hyaloid artery extended to the posterior lens capsule membrane. Like the DV and sinusoidal anastomoses, the hyaloid artery is also a component of the neonatal vasculature that resolves early in development (38). Anomalies in the vascular architecture of *Ah* −/− mice were not limited to the liver and the hyaloid artery. *Ah* −/− mice had an exaggerated limbal vasculature with loops that extend centrally and invade the corneal stroma (Fig. 7*B*). Unfortunately, there have been no reports of the development of the limbal vasculature that would allow us to conclude that this phenomenon is related to those cited above. We also observed that when kidneys were perfused with resin retrograde from the renal vein and out the renal artery, there was an alteration in vascular architecture (Fig. 7*D*). The physiological explanation of the renal defect has not yet been examined thoroughly. Importantly, not all neonatal vascular structures persist in the *Ah* −/− mouse. For example, the ductus arteriosus, a fetal vessel that connects the left pulmonary artery with the descending aorta, was closed in adult *Ah* −/− mice (data not shown), and thus its resolution may be governed by an independent mechanism (39).

Discussion

These data identify the *Ah* locus as the first gene reported to be associated with patent DV, a condition that can be congenital in humans (40, 41) and in dogs (42). These results also provide evidence that the AHR plays a role in the resolution of a number of vascular structures. This aspect of vascular development has been referred to as "pruning," a process by which early vessels are removed to form a more mature vascular pattern (43). Interestingly, other members of the PAS family are involved in angiogenesis, which involves the "sprouting" of vascular structures, an opposing aspect of vascular development (44–48). For example, murine embryos deficient in HIF1α or its partner, ARNT, do not develop past embryo day 11 (44, 47, 48). The underlying mechanism for the *Hif1*α and *Arnt* null phenotypes appears to be related to the inability of the embryos to form the HIF1α/ARNT complexes that mediate the hypoxia-driven transcriptional responses essential for normal developmental angiogenesis (49). Taken together, there appears to be an opposing physiological relationship between the HIF1α and AHR in vascular development, analogous more to "forward" and "reverse" gears than to an "accelerator" and "brake." These opposing roles may govern the development and resolution of certain vascular structures and might provide the background and experimental systems that ultimately lead to an elucidation of the AHR's role in mammalian development.

There are a number of potential mechanisms by which the AHR could play a role in the resolution of vascular structures. Given the AHR's known activity as a transcription factor, it seems likely that it is required for the appropriate regulation of genes involved in vascular remodeling. Although the identity of these genes is unknown, it is tempting to speculate that such gene products are among the battery of genes most known for their role in xenobiotic metabolism (e.g., *Cyp1a1, Cyp1a2, Cyp1b1*, etc.). In such a scenario, one or more of these enzymes could control the levels of low-molecular-weight molecules with roles in vascular resorption. Alternatively, the AHR could influence vascular development by influencing the signaling of other PAS family members that are known to be involved in angiogenesis, such as HIF1α (49, 50). Any of these mechanisms might be influenced by anthropogenic or putative endogenous ligands of the AHR. From a physiological perspective, an endogenous ligand could be a primary signal in the remodeling of vascular structures. From a toxicological viewpoint, these data suggest that an examination of AHR agonist, like dioxin, should be extended to aspects of vascular development.

This work was supported by the Burroughs Wellcome Fund and the National Institutes of Health (ES06883, CA22484, CA07175). G.L. was supported by an individual National Research Service Award (F32 ES05877). R.T. was supported by a National Research Service Award (T32 CA09681) and by a Society of Toxicology Colgate Palmolive Postdoctoral Fellowship. We also thank Henry Pitot and W. Frederick Lahvis for their respective expertise in liver pathology and medical diagnosis.

1. Hoffman, E. C., Reyes, H., Chu, F. F., Sander, F., Conley, L. H., Brooks, B. A. & Hankinson, O. (1991) *Science* **252,** 954–958.
2. Burbach, K. M., Poland, A. & Bradfield, C. A. (1992) *Proc. Natl. Acad. Sci. USA* **89,** 8185–8189.
3. Dolwick, K. M., Swanson, H. I. & Bradfield, C. A. (1993) *Proc. Natl. Acad. Sci. USA* **90,** 8566–8570.
4. Ema, M., Sogawa, K., Watanabe, N., Chujoh, Y., Matsushita, N., Gotoh, O., Funae, Y. & Fujii-Kuriyama, Y. (1992) *Biochem. Biophys. Res. Commun.* **184,** 246–253.
5. Reyes, H., Reisz-Porszasz, S. & Hankinson, O. (1992) *Science* **256,** 1193–1195.
6. Eisen, H. J., Hannah, R. R., Legraverend, C., Okey, A. B. & Nebert, D. W. (1983) *Biochem. Actions Horm.* **10,** 227–257.
7. Telakowski-Hopkins, C. A., King, R. G. & Pickett, C. B. (1988) *Proc. Natl. Acad. Sci. USA* **85,** 1000–1004.

8. Pitot, H. C., Goldsworthy, T., Campbell, H. A. & Poland, A. (1980) *Cancer Res.* **40,** 3616–3620.
9. Holsapple, M. P., Morris, D. L., Wood, S. C. & Snyder, N. K. (1991) *Annu. Rev. Pharmacol. Toxicol.* **31,** 73–100.
10. Shen, E. S., Elferink, C. J. & Whitlock, J. P., Jr. (1991) *Methods Enzymol.* **206,** 403–408.
11. Huuskonen, H., Unkila, M., Pohjanvirta, R. & Tuomisto, J. (1994) *Toxicol. Appl. Pharmacol.* **124,** 174–180.
12. Hahn, M. E., Poland, A., Glover, E. & Stegeman, J. J. (1994) *Arch. Biochem. Biophys.* **310,** 218–228.
13. Jain, S., Maltepe, E., Lu, M. M., Simon, C. & Bradfield, C. A. (1998) *Mech. Dev.* **73,** 117–123.
14. Abbott, B. D., Probst, M. R., Perdew, G. H. & Buckalew, A. R. (1998) *Teratology* **58,** 30–43.
15. Kuchenhoff, A., Seliger, G., Klonisch, T., Tscheudschilsuren, G., Kaltwasser, P., Seliger, E., Buchmann, J. & Fischer, B. (1999) *Fertil. Steril.* **71,** 354–360.
16. Fernandez-Salguero, P., Pineau, T., Hilbert, D. M., McPhail, T., Lee, S. S., Kimura, S., Nebert, D. W., Rudikoff, S., Ward, J. M. & Gonzalez, F. J. (1995) *Science* **268,** 722–726.
17. Schmidt, J. V., Su, G. H.-T., Reddy, J. K., Simon, M. C. & Bradfield, C. A. (1996) *Proc. Natl. Acad. Sci. USA* **93,** 6731–6736.
18. Mimura, J., Yamashita, K., Nakamura, K., Morita, M., Takagi, T. N., Nakao, K., Emak, M., Sogawa, K., Yasuda, M., Katsuki, M., *et al.* (1997) *Genes Cells* **2,** 645–654.
19. Lahvis, G. P. & Bradfield, C. A. (1998) *Biochem. Pharmacol.* **56,** 781–787.
20. Abbott, B. D., Schmid, J. E., Pitt, J. A., Buckalew, A. R., Wood, C. R., Held, G. A. & Diliberto, J. J. (1999) *Toxicol. Appl. Pharmacol.* **155,** 62–70.
21. Elias, H. & Hyde, D. M. (1983) *A Guide to Practical Stereology* (Karger, New York).
22. Cowper, K. B., Currin, R. T., Dawson, T. L., Lindert, K. A., Lemasters, J. J. & Thurman, R. G. (1990) *Biochem. J.* **266,** 141–147.
23. McCuskey, R. S. (1993) in *Optical Microscopy: Emerging Methods and Applications* (Academic, San Diego), pp. 355–372.
24. Chojkier, M. & Groszmann, R. J. (1981) *Am. J. Physiol.* **240,** G371–G375.
25. Agresti, A. (1992) *Stat. Sci.* **7,** 131–135.
26. Fernandez-Salguero, P. M., Hilbert, D. M., Rudikoff, S., Ward, J. M. & Gonzalez, F. J. (1996) *Toxicol. Appl. Pharmacol.* **140,** 173–179.
27. Peters, J. M., Narotsky, M. G., Elizondo, G., Fernandez-Salguero, P. M., Gonzalez, F. J. & Abbott, B. D. (1999) *Toxicol. Sci.* **47,** 86–92.
28. Karn, I., Lynch, S. & Svanas, G. (1987) *Hepatology* **7,** 362–366.
29. Francavilla, A., Ove, P., Polimeno, L., Coetzee, M., Makowka, L., Barone, M., Van Thiel, D. H. & Starzl, T. E. (1988) *Transplant. Proc.* **20,** 494–497.
30. Kawasaki, S., Makuuchi, M., Ishizone, S., Matsunami, H., Masaru, T. & Kawarazaki, H. (1992) *Lancet* **339,** 580–581.
31. Harrison, M. (1953) *Biochem. J.* **55,** 204–211.
32. Uhal, B. D. & Roehrig, K. L. (1982) *Biosci. Rep.* **2,** 1003–1007.
33. Dubuisson, L., Bioulac-Sage, P., Bedin, C. & Balabaud, C. (1984) *J. Submicrosc. Cytol.* **16,** 283–287.
34. Schroder, R., Muller, O. & Bircher, J. (1985) *J. Hepatol.* **1,** 107–123.
35. Healey, J. E. (1970) *Ann. N.Y. Acad. Sci.* **170,** 8–17.
36. Pons, H. A., Morgan, J. S., Hutchinson, M., Rojkind, M., Groszmann, R. J. & Stadecker, M. J. (1989) *Am. J. Trop. Med. Hyg.* **41,** 189–197.
37. McCuskey, R. S., Ekataksin, W., LeBouton, A. V., Nishida, J., Krasovich, M. A., McDonnell, D., Williams, C. & Koldovsky, O. (1997) in *Cells of the Hepatic Sinusoid VI*, eds. Wisse, E., Knook, D. L. & Balabaud, C. (Kupffer Cell Foundation, Leiden), pp. 67–70.
38. Ko, M. K., Chi, J. G. & Chang, B. L. (1985) *J. Pediatr. Ophthalmol. Strabismus* **22,** 188–193.
39. Satoda, M., Zhao, F., Diaz, G. A., Burn, J., Goodship, J., Davidson, H. R., Pierpont, M. E. M. & Gelb, B. D. (2000) *Nat. Genet.* **25,** 42–46.
40. Jacob, S., Farr, G., De Vun, D., Takiff, H. & Mason, A. (1999) *Gut* **45,** 442–445.
41. Uchino, T., Endo, F., Ikeda, S., Shiraki, K., Sera, Y. & Matsuda, I. (1996) *Gastroenterology* **110,** 1964–1968.
42. Schermerhorn, T., Center, S. A., Dykes, N. L., Rowland, P. H., Yeager, A. E., Erb, H. N., Oberhansley, K. & Bonda, M. (1996) *J. Vet. Intern. Med.* **10,** 219–230.
43. Ashton, N. (1966) *Am. J. Ophthalmol.* **62,** 412–435.
44. Kozak, K. R., Abbott, B. & Hankinson, O. (1997) *Dev. Biol.* **191,** 297–305.
45. Maxwell, P. H., Dachs, G. U., Gleadle, J. M., Nicholls, L. G., Harris, A. L., Stratford, I. J., Hankinson, O., Pugh, C. W. & Ratcliffe, P. J. (1997) *Proc. Natl. Acad. Sci. USA* **94,** 8104–8109.
46. Carmeliet, P., Dor, Y., Herbert, J. M., Fukumura, D., Brusselmans, K., Dewerchin, M., Neeman, M., Bono, F., Abramovitch, R., Maxwell, P., *et al.* (1998) *Nature (London)* **394,** 485–490.
47. Kotch, L. E., Iyer, N. V., Laughner, E. & Semenza, G. L. (1999) *Dev. Biol.* **209,** 254–267.
48. Maltepe, E., Schmidt, J. V., Baunoch, D., Bradfield, C. A. & Simon, M. C. (1997) *Nature (London)* **386,** 403–407.
49. Maltepe, E. & Simon, M. C. (1998) *J. Mol. Med.* **76,** 391–401.
50. Gu, Y.-Z., Hogenesch, J. & Bradfield, C. (2000) in *Annu. Rev. Pharmacol. Toxicol.* (Academic Press), 519–561.